

## Unstable growth of bubbles from a constriction

Marc Grosjean  and Elise Lorenceau *Université Grenoble Alpes, CNRS, LIPhy, F-38000 Grenoble, France*

(Received 9 January 2023; accepted 3 April 2023; published 22 May 2023)

Bubbles and droplets are ubiquitous in many areas of engineering, including microfluidics where they can serve as microreactors for screening of chemical reactions. They are often formed out of a constriction (a microfluidic channel or a cylindrical tube) by blowing a given volume of gas into a liquid phase. It is obviously crucial to be able to control their size, which is not always easy due to the coupling between the volume of the bubble and the gas pressure induced by the Laplace law. In this paper, we examine the size and formation dynamics of soap bubbles blown from a cylindrical tube, which is the paradigm geometry for bubble and droplet formation. To do so, one end of the tube is closed by a soap film, while the other end is connected to a large reservoir of variable volume filled with gas. To inflate the bubble, we reduce the volume of the reservoir, which mimics air inflation through the lung diaphragm or the flow-rate-driven bubble formation in microfluidics geometry such as flow-focusing. As the volume of the reservoir decreases, the soap film curves and takes the form of a spherical cap with a smaller and smaller radius of curvature, which leads to the increase of the gas pressure in the reservoir, according to Laplace's law. This quasistatic process continues until a critical pressure is reached for which the bubble is quasi-hemispherical. Beyond this pressure, the film undergoes a rapid topological transformation and swells very rapidly (in less than 100 ms) until it reaches its final volume. We describe this instability in particular by showing that this unstable regime appears when a dimensionless number, which depends on the volume of the reservoir, the radius of the tube, surface tension, and external pressure, reaches a critical value. Using a quasistatic model that we solve analytically, we predict the bubble growth dynamics and the amplitude of the unstable height increase for any reservoir volume and constriction size.

DOI: [10.1103/PhysRevFluids.8.053602](https://doi.org/10.1103/PhysRevFluids.8.053602)

### I. INTRODUCTION

Among the successes of microfluidics is the possibility of forming large assemblies of drops or bubbles almost identical at high throughput (of the order of 100 Hz) [1–3]. These entities, dispersed in a continuous liquid phase and used as microreactors containing active ingredients at a concentration changing from drop to drop, allows analysis and screening of chemical reactions with unprecedented throughput [4–7]. Bubbles and drops are also found in other fields of engineering where they are generally dispersed in a continuous liquid phase, themselves then being qualified as the dispersed phase (fire-fighting foam or sparkling drinks [8]). There are many methods to make monodisperse bubbles or drops such as shearing crude emulsion to split it into tiny droplets [9,10] or blowing on an interface [11–13]. One commonly used in microfluidics and called flow-focusing consists in forming bubbles (or drops) by deforming an air-liquid interface placed at the end of a tube (of square, rectangular, or circular section) from a reservoir whose pressure increases [1]. In the dripping regime, three distinct steps can be identified: (1) a phase of quasistatic deformation of the interface fixed to the end of the tube which, by bending, changes from a flat geometry to that

of a quasihemispherical cap with a radius equal to that of the tube; (2) a rapid growth (generally in less than 100 milliseconds) of this hemisphere until reaching a final almost spherical shape of radius much greater than that of the tube; (3) finally, pinch-off regime with detachment of the bubble from the constriction [14,15]. Depending on the geometry of the system used, gravity or viscous friction forces produce the work necessary to stretch the neck separating the spherical bubble to the point of spontaneous rupture driven by capillary forces [16,17]. When nothing comes to disturb the bubble, it remains attached to the end of the constriction or the tube, as illustrated by several paintings representing children having blown bubbles, the most known being those of J. S. Chardin or E. Manet [18].

To obtain the most-peaked bubble-size distribution, the time of the pinch-off regime (3), which is intrinsically variable as a result of hydrodynamic instability, must be much shorter than the time of growth regimes (1) and (2). Thus, the pinching dynamics of fluid necks have been studied with great care, revealing the importance of convection [14,19], swirl [20], confinement [21], and presence of surfactants or not [22]. On the contrary, the dynamics of phases (1) and (2) have been much less explored, the implicit hypothesis being that the duration of this phase is controlled by the flow rate of the dispersed phase and the volume of the bubble at the threshold of breakup. However, what sets this flow rate is not always obvious. For pressure-driven flow of the dispersed phase, nonlinear variations of the gas flow rate, induced by hydrodynamic feedback in the outlet channel, have been reported in several studies [23–25]. For flow-rate-driven flow, this difficulty should not exist, yet we reveal in this work that the compliance of the system—which arises here from the gas compressibility—induces a mechanical coupling between the deformation of the interface at the constriction and the pressure in the gas reservoir. This coupling can induce large fluctuations in the flow rate that lead to unstable bubble formation modes. We therefore study the first steps of bubble growth at an imposed flow rate in a geometry reminiscent of the one used by children when they blow a bubble from a tube. By comparing experimental results with an analytical model, we predict the final bubble volume. In particular, we show that the initial volume of the reservoir comprising the gas—usually not considered—is a key parameter of this process.

## II. EXPERIMENT

The soap film is made of a mixture of Sodium Dodecyl Sulfate (SDS) at a concentration of 24 mmol/L, which is 3 times larger than the CMC, 20% of glycerine and deionized water. The solution is used at least 3 days after it has been made to ensure that the hydrolysis of SDS into dodecanol is achieved [26]. The liquid/air surface tension,  $\gamma$ , is measured prior to any experiment using the pendant drop technique [27] and we systematically found  $\gamma = 23 \pm 2$  mN/m. The soap film is deposited at the extremity of a tube of external radius,  $a$ , ranging between 0.3 and 0.83 mm. The other extremity of the tube is connected to a reservoir composed of two syringes of volumes  $V_1$  and  $V_2$  (see Fig. 1). The total volume of the reservoir  $V$ —which includes  $V_1$ ,  $V_2$ ,  $V_d$  the dead volume of the valve and the tube and  $\Omega$  the volume comprised between the film and the outlet of the tube—varies between 1 and 50 mL. A first syringe, connected to a syringe pump (KdScientific), is used to reduce the volume of the reservoir at a flow rate  $-dV_1/dt = Q$ , with  $Q$  equal to 1 or 2  $\mu\text{L/s}$ . A second syringe serves to change the initial total volume of the reservoir  $V(t=0) = V_0$ . The deformation of the soap film is monitored by a camera Marlin from Allied Vision.

At  $t = 0$ , the syringe pump and the camera are triggered simultaneously (the error associated with this manual triggering is estimated at less than one second). The reduction of the volume of the reservoir increases the pressure and bends the soap film. The liquid film is much softer than the rest of the elements containing the compressed gas (syringe tube and connectors), then we assume that only the film is deformable. To avoid premature rupture of the soap film, a transparent plastic box is placed around the bubble to limit its evaporation. This allows an easy observation of stable bubbles for several minutes. We made sure that this plastic box is not completely airtight so that the external pressure around the bubble is the atmospheric pressure.

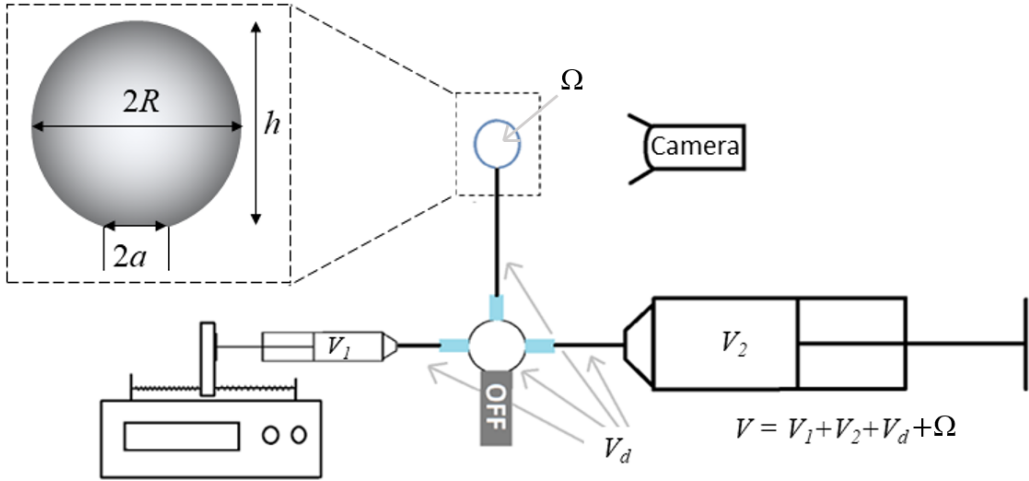


FIG. 1. Experimental setup: the bubble of radius of curvature  $R$  and height  $h$  is connected to a large reservoir of volume  $V$  constituted by the volume of the two syringes,  $V_1$  and  $V_2$ , the dead volume of the connectors  $V_d$  and the volume of the spherical cap,  $\Omega$ , of the bubble. The volume  $V_1$  is decreased at a flow rate  $Q$  thanks to a syringe pump.

### III. EXPERIMENTAL RESULTS

In our experiments, we have observed that two clearly different regimes of bubble inflation exist, a quasistatic one and a second that is highly dynamic. Those two regimes are illustrated in Figs. 2(a) and 2(b). In both cases  $V_0$  is identical while  $a$  is 2.8 times bigger in Fig. 2(b) than in Fig. 2(a). The bubble in Fig. 2(b), swelled from a large tube, continuously inflates step by step while the swelling of the bubble in Fig. 2(a) is unstable and takes place in less than 5 ms. To go further, we report in Fig. 3 the evolution of  $h$ , the height of the bubble, defined in Fig. 1, as a function of time,  $t$ , at the same flow rate and radius but for different  $V_0$ . As we can see, we can make a distinction between the two regimes, a first for  $V_0 < 10$  ml where the growth of the bubble is continuous and a second for  $V_0 \geq 10$  ml, where the swelling is unstable. In this second regime, the curves are S-shaped with a near-vertical zone meaning that the height of the bubble,  $h$ , changes from one to several millimeters in less than 5 ms.

The nonmonotonic evolution of the radius of curvature,  $R$ , of the soap film is a crucial point to explain the distinction of regime observed in experiment. This radius is both constrained by

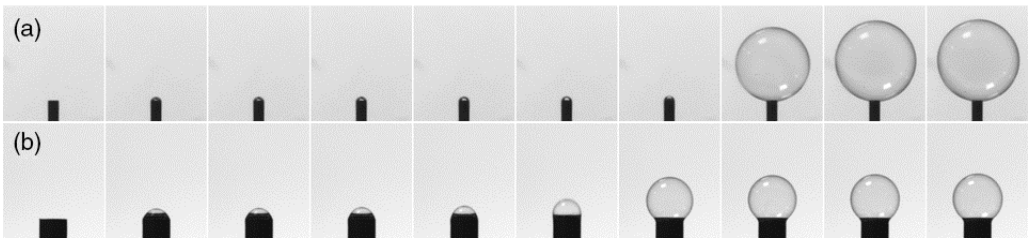


FIG. 2. Sequences of image showing two bubbles blown from reservoirs of identical volume  $V_0 = 10$  mL. In a)  $a = 0.3$  mm and in b)  $a = 0.83$  mm. The thumbnails are separated by 5 ms except for the first ones which show the tube before the start of soap film compression.  $Q = 2 \mu\text{L/s}$  in a) and  $Q = 1 \mu\text{L/s}$  in b) so that both inflations take place in the same time frame.

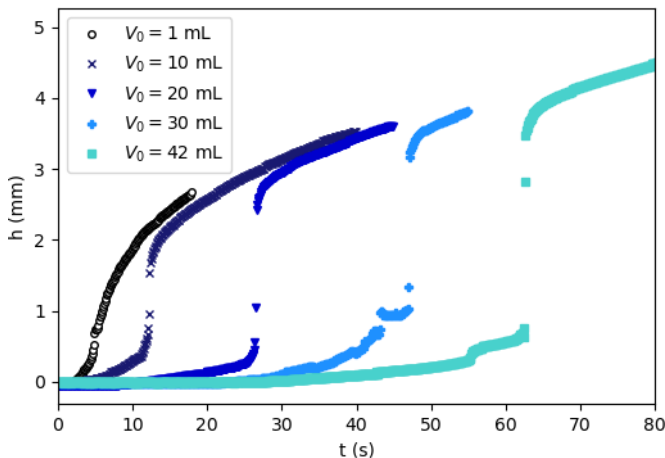


FIG. 3. Height of the bubble,  $h$ , as a function of time,  $t$ , for  $a = 0.83$  mm,  $Q = 2 \mu\text{L/s}$ , and different  $V_0$ . For  $V_0 = 42, 30$ , and  $20$  mL, the bubble inflation is unstable while for  $V_0 = 1$  and  $10$  mL, it is continuous. For each curve, the time origin is adjusted so that the data collapses at long times. The recording of the different curves is stopped just before the explosion of the bubbles due to the thinning of the soap film over time.

$a$ , the radius of the tube, and the evolution of the pressure,  $P$ , which follows the Laplace's law  $P = P_0 + 4\gamma/R$ , where the factor 4 arises from the presence of two liquid/air interfaces.

At first, the pressure in the reservoir is identical to the atmospheric pressure and the film is flat, thus  $R \rightarrow \infty$ . When the volume of the reservoir decreases due to the syringe pump, the pressure increases. The soap film then bends,  $R$  decreases and Laplace-over pressure increases accordingly. However, due to geometrical constraint,  $R$  cannot reach a value smaller than  $a$  which corresponds to a maximal pressure  $P^* = P_0 + 4\gamma/a$ . At this point, any further compression of  $V$  by the syringe pump triggers an instability because the overpressure in the reservoir can no longer be balanced by Laplace's law since the radius of curvature of the bubble has reached its minimum value  $a$  and can no longer decrease. The bubble is now in a nonequilibrium state in which compressed air has been stored in the reservoir. To regain a state of equilibrium, the bubble inflates very quickly until Laplace's law relating internal and external pressure of the bubble to the radius of curvature of the interface is verified again. The characteristic time of this inflation is very short, totally independent of the speed of the syringe pump, and depends on the amount of compressed air stored. Afterwards, any further compression by the syringe pump is compensated by an increase in the size of the bubble.

#### IV. MODEL

To understand these results, we write simple thermodynamic arguments stemming from the conservation of  $n$ , the number of gas moles in the reservoir. This is valid if the whole system is gas tight, hence if the rate of mole transfer  $dn/dt$  due to the permeability  $k$  of the soap film is negligible. From Fick's law,  $dn/dt = -kA\Delta C$ , where  $k$  is the soap film permeability,  $A \approx 4\pi R^2$  the area of the bubble and  $\Delta C$  the difference of gas concentration between the reservoir and the atmosphere surrounding the bubble. Using  $R \sim 1$  mm,  $k \sim 1$  mm/s, a typical value from literature for SDS surfactants without salts [28,29], and  $\Delta C = 4\gamma/(RR_uT_0)$ , where  $R_u = 8.31$  J/mol/K is the universal gas constant and  $T_0 = 298$  K and  $P_0 = 1$  atm, the ambient temperature and pressure, we find  $dn/dt \sim 2 \times 10^{-10}$  mol/s. As the bubble typically forms in 100 s, the variation of moles in the bubble due to the permeability of the soap film is  $\delta n \sim 2 \times 10^{-8}$  mol. This is very small when compared to  $n_0 = P_0V_0/(R_uT_0) \approx 1.2 \times 10^{-3}$  mol, thus we assume the system to be air tight and consider  $n$  to be constant. Writing the conservation of  $n$  for a polytropic transformation, i.e.,

$PV^k = P_0V_0^k$ , where  $k$  is a constant ( $k = 1$  for isothermal,  $k = 0$  for isobaric,  $k = \infty$  for isochoric and  $k =$  heat capacity ratio for isentropic transformations) yields

$$1 = \left(1 + \frac{4\gamma}{P_0R}\right) \left(1 + \frac{\Omega}{V_0} - \frac{Qt}{V_0}\right)^k, \quad (1)$$

where  $\Omega = \pi h/2(a^2 + \frac{h^2}{3})$  is the volume of the spherical cap, that is expressed as a function of  $a$ , the tube radius, and  $h$  is the height of the spherical cap (see Fig. 1). Since  $R > a$ , with  $a$  ranging between 0.3 and 0.83 mm,  $\frac{4\gamma}{RP_0} < \frac{4\gamma}{aP_0} \ll 1$ , we make a Taylor expansion of Eq. (1) and express the geometrical quantities  $\Omega$  and  $R$  as a function of  $h$  using the geometrical relation  $2hR = h^2 + a^2$ . We also introduce the dimensionless parameters  $x = h/a$ ,  $\tau = \frac{2Qt}{\pi a^3}$  which are made dimensionless by using the tube radius as the characteristic length and the time to fill a volume proportional to  $a^3$  at  $Q$  as the characteristic time. This choice as well as that of the factor  $2/\pi$  arises naturally from the equations, so that Eq. (1) finally writes

$$\tau = x \left(1 + \frac{x^2}{3}\right) + \frac{Bx}{x^2 + 1}, \quad (2)$$

with  $B = \frac{16\gamma V_0}{\pi k a^3 P_0}$  comparing the Laplace pressure  $\gamma/a$  to the atmospheric pressure  $P_0$  and the initial volume of the reservoir  $V_0$  to  $a^3$ . In Fig. 4, the numerical solution of Eq. (2) is plotted for different values of  $B$ . Two types of bubble growth are observed: for small values of  $B$ ,  $x$  increases as  $\tau$  increases and the bubble formation is monotonic and proceeds continuously accordingly with the observations of Figs. 2 and 3, which revealed continuous bubble formation for large values of  $a$  and small values of  $V_0$ . For larger values of  $B$  (typically  $B \geq 38$  on Fig. 4), the curves corresponding to the numerical solution of Eq. (2) are S-shaped with nonmonotonic variation of  $\tau$  as a function of  $x$ , which is not physical since  $\tau$  - the dimensionless time - should always increases. Thus, when  $d\tau/dx$  is negative, there is no physical solution to the equation, and the dimensionless height suddenly jumps from one value to another. In the following, we call  $x_1$  the maximum value of  $x$  before the jump and  $x_2$  the minimum value of  $x$  after the jump. The numerical solutions is also compared with the experimental data of Fig. 3. For the latter, the data are made dimensionless using the experimental parameters as described before and  $B$  is calculated assuming an isothermal ( $k = 1$  and  $B = B_i$ ) or an adiabatic transformation ( $k = C_p/C_v = 1.4$  and  $B = B_a$ ). Here, we recall that there is an experimental uncertainty on the initial time. It is therefore not the temporal position of the jump but rather its amplitude that must be considered. We observe that the agreement between the experimental data and the model is slightly better for the isothermal transformation than for the adiabatic one since the amplitude of the experimental jump is better described by the theoretical curves with the value of  $B$  equal to  $B_i$  rather than  $B_a$ .

We now determine  $x_1$  and  $x_2$  as follows. We first calculate  $x_1$ , the dimensionless height at the onset of the formation of an unstable bubble, for which  $\frac{d\tau}{dx}|_{x=x_1} = 0$ . Hence,  $x_1$  is a solution of

$$B^{-1}(1 + x^2)^3 - x^2 + 1 = 0. \quad (3)$$

Using  $X = 1 + x^2$ , Eq. (3) can be reduced to a polynomial of degree 3:

$$B^{-1}X^3 - X + 2 = 0. \quad (4)$$

We seek for solutions larger than one using the Cardan method [30]. For  $B \leq 27$ , there is no real solution larger than one for Eq. (4), hence  $\frac{d\tau}{dx} > 0$  and the formation of the bubble is continuous.

For  $B \geq 27$ , two real solutions exist, but only one,  $X_1$ , is larger than one, increases with  $B$ , and is physically consistent when  $B \rightarrow \infty$ :

$$X_1 = 2\sqrt{\frac{B}{3}} \cos \left[ \frac{1}{3} \arccos \left( -3\sqrt{\frac{3}{B}} \right) + \frac{4\pi}{3} \right]. \quad (5)$$

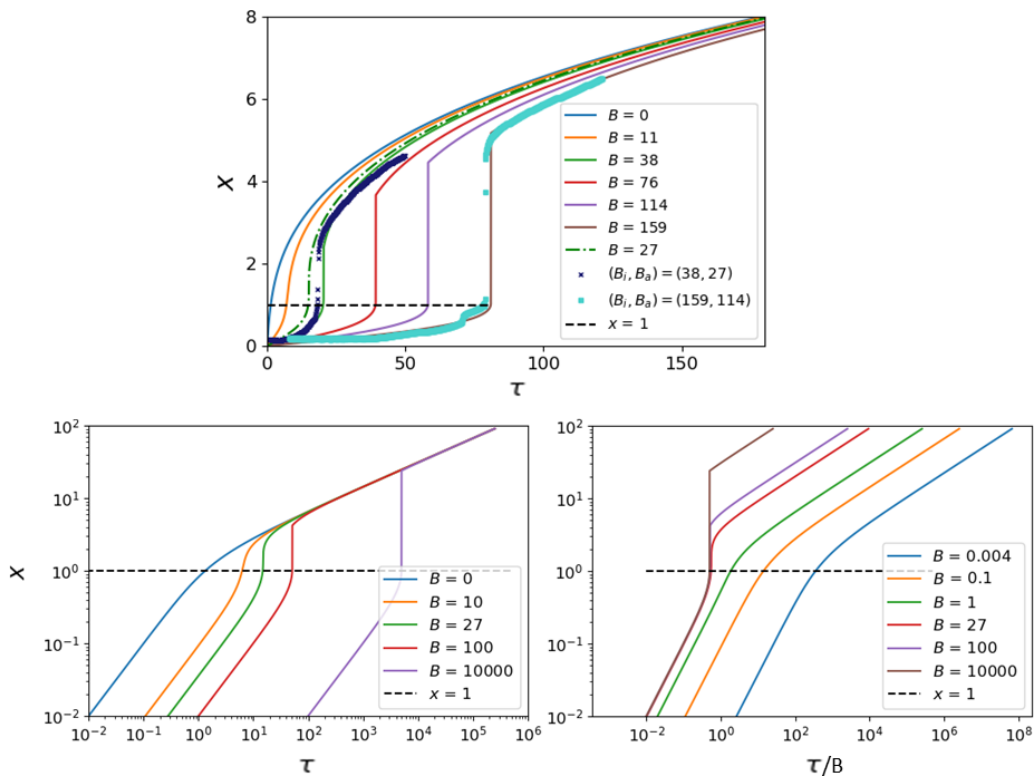


FIG. 4. Top: Dimensionless height  $x$  as a function of dimensionless time  $\tau$  in lin/lin scale. The lines correspond to theoretical data for different values of  $B$  calculated using Eq. (2). Two regimes are observed: for  $B \leq 27$ ,  $x$  is defined unequivocally as a function of  $\tau$  and the slope  $dx/d\tau$  always reaches a finite value, whereas for  $B > 27$ ,  $x$  is multivalued and the slope  $dx/d\tau$  reaches an infinite value. The dashed-dotted curve corresponds to  $B = 27$ . The points correspond to experimental data of Fig. 3 which have been made dimensionless ( $V_0 = 10$  and 42 ml). For each experimental curve, the equivalent  $B$  is calculated assuming an isothermal expansion  $B_i$  or an adiabatic expansion  $B_a$ , hence taking  $k = 1$  or  $k = 1.4$ . Bottom left: dimensionless height  $x$  as a function of dimensionless time  $\tau$  in log/log scale for various  $B$ . Bottom right: dimensionless height  $x$  as a function of  $\tau/B$  for various  $B$ .

Thus, the instability is triggered, as soon as  $x > x_1$ , where  $x_1 = \sqrt{X_1 - 1}$ , with  $X_1$  given by Eq. (5).

To determine  $x_2$ , the dimensionless height of the bubble after the unstable swelling, we assume that the swelling is instantaneous and write  $\tau(x_1) = \tau(x_2)$  using Eq. (2). This leads to a fourth-order polynomial equation in  $x_2$ :

$$x_2^4 + x_1 x_2^3 + (x_1^2 + 4)x_2^2 + x_1 \left(1 - \frac{3B}{x_1^2 + 1}\right)x_2 + 3 + x_1^2 + \frac{3B}{x_1^2 + 1} = 0. \quad (6)$$

Since  $x_1$  is also a solution of Eq. (6) we factorize by  $(x_2 - x_1)$  to reduce the polynomial of degree 4 to a polynomial of degree 3:

$$x_2^3 + 2x_1 x_2^2 + (4 + 3x_1^2)x_2 - \left(\frac{3B}{x_1(1 + x_1^2)} + \frac{3}{x_1} + x_1\right) = 0. \quad (7)$$

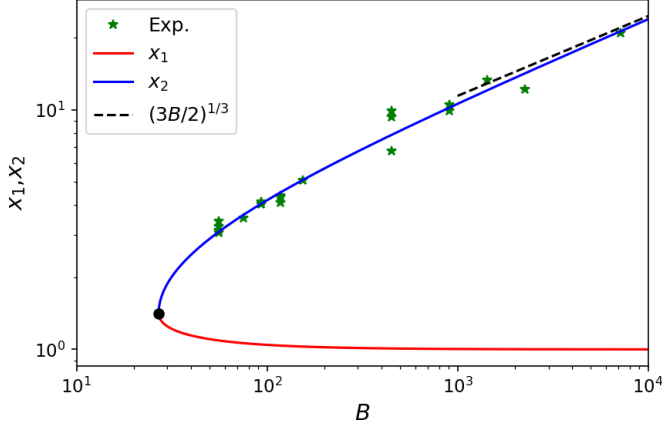


FIG. 5. Analytical solutions  $x_1$  of Eq. (5) and  $x_2$  of Eq. (7) as a function of  $B$ . The two curves meet for  $B = 27$  at  $x_1 = x_2 = \sqrt{2}$ . For  $B < 27$ ,  $x_1$  and  $x_2$  are not defined as the bubble inflates continuously. For  $B \rightarrow \infty$ ,  $x_1 \rightarrow 1$  and  $x_2 \sim (\frac{3}{2}B)^{1/3}$ . The green stars correspond to experimental data assuming an isothermal expansion.

Equation (7) can also be solved analytically after a change of variable  $X_2 = x_2 + \frac{2x_1}{3}$  and using the Cardan method [30], which leads to

$$X_2 = \sqrt[3]{\frac{1}{2}\left(-q + \sqrt{\frac{D}{27}}\right)} - \sqrt[3]{\frac{1}{2}\left(q + \sqrt{\frac{D}{27}}\right)}, \quad (8)$$

with  $D = 27q^2 + 4p^3$ ,  $q = \frac{43}{27}x_1^3 + \frac{63}{27}x_1 - \frac{3Bx_1}{(1+x_1^2)}$ , and  $p = \frac{5}{3}x_1^2 + 4$ .  $x_1$  and  $x_2$  are plotted as a function of  $B$  in Fig. 5 and discussed in the following section.

## V. RESULTS

We now discuss the outcomes of the model. In Fig. 5, we plot the simple analytical expressions of  $x_1$  and  $x_2$  as a function of  $B$ . For  $B < 27$ ,  $x_1$  and  $x_2$  are not defined and the bubble growth proceeds continuously. For  $B = 27$ , Eqs. (5) and (8) ensure  $X_1 = 3$  and  $X_2 = \frac{5}{3}\sqrt{2}$ , hence  $x_1 = x_2 = \sqrt{2}$ , as highlighted by the black dot of coordinate  $(27, \sqrt{2})$ , which superimposes with the two curves of Fig. 5. For  $B \rightarrow \infty$ , several points are worth discussing. First, before the instability ( $x \ll 1$ ), it is the second term of equation 2 that is dominant. In this limit of small  $x$  but large  $B$ ,  $\tau \sim Bx$  as revealed by the good collapse of the data for  $B > 27$  in log/log scale when plotting  $x$  as a function of  $\tau/B$  (see Fig. 4 bottom right). Then, above the instability ( $x \gg 1$ ), it is the first term of Eq. (2) that is dominant. In this limit of large  $x$  and large  $B$ ,  $\tau \sim x^3/3$  has revealed by the collapse of the data in log/log scale when plotting  $x$  as a function of  $B$  (see Fig. 4 bottom left). Last, Eq. (3) gives  $x_1 \rightarrow 1$  as observed in Fig. 5. Since  $B$  increases with  $V_0$  and decreases with  $a$ , this suggests that for large  $V_0$  and/or small  $a$ , the instability is triggered as soon as  $h \rightarrow a$ , hence when the bubble reaches a shape akin to a hemisphere in agreement with the Laplace pressure limit set by the radius of the tube. Then imposing  $x_1$  in Eq. (7) yields to  $x_2 \sim (\frac{3}{2}B)^{1/3}$ . In this asymptotic limit, which correctly reproduces the full calculation of  $x_2$  for  $B \geq 10^3$  as highlighted by the dashed line in Fig. 5, the height of the bubble at the end of the instability is of the order of  $a(\frac{3}{2}B)^{1/3}$ . In this limit of large  $B$ , the bubble is quasispherical and its volume  $\Omega$  right after the jump is  $\Omega = \frac{\pi}{6}h^3$ . Therefore, our model predicts that the bubble volume after the instability is equal to  $V_0 \frac{4\gamma}{aP_0}$ , which is surprisingly proportional to  $V_0$  the volume of compressed gas upstream of the constricted zone modulated by the ratio of the Laplace pressure over the atmospheric pressure.

The comparison of the theoretical values of  $x_1$  and  $x_2$  with the experimental data is not immediate for the following reasons. First, the determination of  $ax_1$ , the height of the bubble at the onset of the instability is delicate due to the small range of variation of  $x_1$ , so we do not propose experimental data points on Fig. 5 concerning  $x_1$ . Second, the data of Fig. 3 shows a very fast growth of the bubble, but not instantaneous. Thus, to experimentally extract the height  $ax_2$  corresponding to the end of the instability, we use the following arbitrary criterion: the bubble is in the unstable mode as soon as  $dh/dt$  is greater than  $af$  where  $f$  is the acquisition frequency of the camera. Despite this arbitrary criterion, the corresponding experimental data show a remarkable agreement with the model as illustrated in Fig. 5. The model thus confirms the importance of  $V_0$  and  $a$  for bubble sizing and gives a direct relation between those parameters which could have direct application in microfluidic engineering processes.

## VI. DISCUSSION

The system we describe—namely, ejection of a large volume of gas when the pressure in the microfluidic reservoir exceeds a critical value—is analogous to what could be observed when following the volume of gas ejected from a macroscopic pressure cooker equipped with a weighted valve. In these cookers, the charging phase where the pressure increases in the cooker is contained by the weight of the valve, is followed by a discharging phase, where a large volume of gas is ejected very quickly when the pressure exceeds the threshold supported by the valve. Beyond that, the gas flow rate out of the cooker remains constant. In the problem we study, the constriction of the tube,  $a$ , that imposes the maximum capillary pressure that the system can support is then equivalent to the valve of the pressure cooker. Recently, Keiser *et al.* [31] have shown that a similar behavior can also be observed in a dead-end microchannel containing a constriction, initially filled with water. The instability is then driven by the pervaporation of the liquid through the channels. Yet, in their case, the water being incompressible, it is the compliance of the elastic channels that allows the variation of pressure of the water. As for our system, the kinetics of fluid escape depends on the volume under tension. Magdelaine *et al.* [32] who studied a gaseous system very similar to the one considered here where the volume of compressed gas ejects into water rather than into a bubble, also highlights the importance of the volume of the pressurized reservoir. By adopting a very different formalism from ours and introducing the pinching kinetics of the gas jet ejected into the water, they produce a comprehensive model predicting the number of bubbles formed during the compression of a gaseous syringe. Overall, in these two-phase systems, it is the compliance of the system, whether it comes from the compressibility of the gas or the elasticity of the microfluidic channels, which is at the origin of this instability as thoroughly discussed in Ref. [33] for two-phase microfluidics flow.

In view of these results, two points seem interesting to discuss.

The first point of interest concerns the formation of monodisperse bubbles in microfluidic geometries where the interface is confined in a constriction, like flow-focusing. Experimentalists in this field are well aware that the bubble-size distributions produced in this type of geometry when the gas phase is flow-rate-driven are more difficult to control and less peaked (with standard deviations higher than 20%) than when the gas is driven at controlled pressure [34]. This explains why pressure-driven gas control is often preferred to flow-rate gas control. Our work sheds light on this point: taking typical values  $a = 100 \mu\text{m}$ ,  $V_0 = 1 \text{ ml}$ , it comes  $B \sim 1000$ , which clearly shows that those devices are in the unstable regime highlighted here. This suggests that the volume of the syringe containing the gas,  $V_0$ , a parameter usually not considered, must be taken into account to set the bubbles size. Moreover, one can ask which transformation (adiabatic or isothermal) is more relevant in microfluidics. The isothermal assumption will be more realistic if the characteristic time of thermal diffusion  $\alpha \sim a^2/\kappa$ , where  $\kappa$  is the heat diffusivity in air ( $\kappa \sim 20 \cdot 10^{-6} \text{ m}^2/\text{s}$  at ambient temperature and pressure) and  $a$  the diameter of the constriction, is smaller than the characteristic time needed to form a bubble, which depends on the geometry of the microfluidic device. For the experiment proposed here, we find  $\alpha \sim 30 \text{ ms}$  which is a bit less than the time needed to produce

a bubble, here of the order of 100 ms, thus suggesting a gaseous expansion closer to an isothermal expansion than to an adiabatic one.

Second, the proposed model, in good agreement with the experiments, allows to predict the unstable growth regime ( $B > 27$ ) as well as the amplitude of this phase, set by  $a(x_2 - x_1)$ . Since it is based on quasistatic arguments, it does not perfectly capture the growth dynamics of the bubble in the unstable regime. Indeed, for  $B > 27$ , we predict that the height  $h/a$  jumps from  $x_1$  to  $x_2$  instantaneously (see Fig. 4), which is neither physical nor confirmed by experiments. As can be seen in Fig. 3, the growth is very fast but not infinite because in practice, this expansion regime is limited by a dissipative process being either inertia of the gas, viscosity of the gas or liquid or rheology of the interface. A detailed follow-up of the bubble growth kinetics using a high-speed camera in the limit where it is limited by the interfacial rheology, seems a promising prospect for this work, since it could open the way to a new characterization of the interfacial rheology of surfactants in a nearly spherical geometry. Indeed, it has been recently shown that “capillary pressure elastometry,” which consists in analyzing the quasistatic pressure-deformation curves for a bubble in this type of geometry, allows to analyze the elastic properties of interfaces [35]. The simple model proposed here should allow to extend the field of application of “capillary pressure elastometry” to the dynamic response of interfaces.

## VII. CONCLUSION

We have shown that the growth of bubbles blown in noncompliant geometries can exhibit unstable regimes. Our experimental and theoretical study reveals the importance of the coupling between the constriction zone on which the interface is anchored and the volume of the reservoir in which the gas is compressed. The use of these unstable regimes to probe elongational interfacial rheology seems to us among the most promising perspective of this work.

## ACKNOWLEDGMENTS

The authors thank J. Giraud for his technical help and L. Keiser, P. Marmottant, B. Dollet, Q. Magdelaine, and A. Antkowiak for fruitful discussions. An anonymous referee is also sincerely thanked for the suggestion concerning the introduction of the  $k$  polytropic parameter. This work is supported by funding from Pack Ambition Recherche 2021 of the region AURA (SELFI project). M.G. designed the research, conducted the experiments, and made the model. M.G. and E.L. discussed the results and wrote the article. There is no conflict to declare.

- 
- [1] S. Anna, N. Bontoux, and H. Stone, Formation of dispersions using “flow focusing” in microchannels, *Appl. Phys. Lett.* **82**, 364 (2003).
  - [2] A. Huerre, V. Miralles, and M.-C. Jullien, Bubbles and foams in microfluidics, *Soft. Matter.* **10**, 6888 (2014).
  - [3] S. L. Anna, Droplets and bubbles in microfluidic devices, *Annu. Rev. Fluid Mech.* **48**, 285 (2016).
  - [4] H. Song, D. L. Chen, and R. F. Ismagilov, Reactions in droplets in microfluidic channels, *Angew. Chem. Int. Ed.* **45**, 7336 (2006).
  - [5] E. Brouzes, M. Medkova, N. Savenelli, D. Marran, M. Twardowski, J. B. Hutchison, J. M. Rothberg, D. R. Link, N. Perrimon, and M. L. Samuels, Droplet microfluidic technology for single-cell high-throughput screening, *Proc. Natl. Acad. Sci. USA* **106**, 14195 (2009).
  - [6] M. T. Guo, A. Rotem, J. A. Heyman, and D. A. Weitz, Droplet microfluidics for high-throughput biological assays, *Lab Chip* **12**, 2146 (2012).
  - [7] J.-C. Baret, Surfactants in droplet-based microfluidics, *Lab Chip* **12**, 422 (2012).
  - [8] P. Stevenson, *Foam Engineering: Fundamentals and Applications* (Wiley, New York, NY, 2012).

- [9] T. G. Mason and J. Bibette, Emulsification in Viscoelastic Media, *Phys. Rev. Lett.* **77**, 3481 (1996).
- [10] J. Bibette, F. LealCalderon, V. Schmitt, and P. Poulin, in *Emulsion Science: Basic Principles—An Overview*, Springer Tracts in Modern Physics, Vol. 181 (Springer, Berlin, 2002), pp. 79–95.
- [11] O. Basaran, Small-scale free surface flows with breakup: Drop formation and emerging applications, *AIChE J.* **48**, 1842 (2002).
- [12] L. Salkin, A. Schmit, P. Panizza, and L. Courbin, Generating Soap Bubbles by Blowing on Soap Films, *Phys. Rev. Lett.* **116**, 077801 (2016).
- [13] C. A. E. Hamlett, D. N. Boniface, A. Salonen, E. Rio, C. Perkins, A. Clark, S. Nyugen, and D. J. Fairhurst, Blowing big bubbles, *Soft Matter* **17**, 2404 (2021).
- [14] P. Garstecki, H. A. Stone, and G. M. Whitesides, Mechanism for Flow-Rate Controlled Breakup in Confined Geometries: A Route to Monodisperse Emulsions, *Phys. Rev. Lett.* **94**, 164501 (2005).
- [15] B. Dollet, W. van Hoeve, J.-P. Raven, P. Marmottant, and M. Versluis, Role of the Channel Geometry on the Bubble Pinch-Off in Flow-Focusing Devices, *Phys. Rev. Lett.* **100**, 034504 (2008).
- [16] J. Eggers, Nonlinear dynamics and breakup of free-surface flows, *Rev. Mod. Phys.* **69**, 865 (1997).
- [17] J. Eggers and E. Villermaux, Physics of liquid jets, *Rep. Prog. Phys.* **71**, 036601 (2008).
- [18] Wikipedia, Les bulles de savon, [https://fr.wikipedia.org/wiki/Les\\_Bulles\\_de\\_savon](https://fr.wikipedia.org/wiki/Les_Bulles_de_savon).
- [19] A. M. Gañán-Calvo, Perfectly monodisperse microbubbling by capillary flow focusing: An alternate physical description and universal scaling, *Phys. Rev. E* **69**, 027301 (2004).
- [20] M. A. Herrada, A. M. Ganán-Calvo, and J. M. López-Herrera, Generation of small mono-disperse bubbles in axisymmetric T-junction: The role of swirl, *Phys. Fluids* **23**, 072004 (2011).
- [21] J. G. Hagedorn, N. S. Martys, and J. F. Douglas, Breakup of a fluid thread in a confined geometry: Droplet-plug transition, perturbation sensitivity, and kinetic stabilization with confinement, *Phys. Rev. E* **69**, 056312 (2004).
- [22] W. van Hoeve, B. Dollet, J. M. Gordillo, M. Versluis, L. van Wijngaarden, and D. Lohse, Bubble size prediction in co-flowing streams, *Europhys. Lett.* **94**, 64001 (2011).
- [23] J.-P. Raven and P. Marmottant, Periodic Microfluidic Bubbling Oscillator: Insight Into the Stability of Two-Phase Microflows, *Phys. Rev. Lett.* **97**, 154501 (2006).
- [24] J. P. Raven, P. Marmottant, and F. Graner, Dry microfoams: formation and flow in a confined channel, *Eur. Phys. J. B* **51**, 137 (2006).
- [25] M. T. Sullivan and H. A. Stone, The role of feedback in microfluidic flow-focusing devices, *Philos. Trans. R. Soc. A* **366**, 2131 (2008).
- [26] V. Bergeron and C. Radke, Equilibrium measurements of oscillatory disjoining pressures in aqueous foam films, *Langmuir* **8**, 3020 (1992).
- [27] A. Daerr and A. Mogne, Pendent drop an ImageJ plugin to measure the surface tension from an image of a pendent drop, *J. Open Res. Softw.* **4**, 3 (2016).
- [28] C. Hadji, B. Dollet, H. Bodiguel, W. Drenckhan, B. Coasne, and E. Lorenceau, Impact of fluorocarbon gaseous environments on the permeability of foam films to air, *Langmuir* **36**, 13236 (2020).
- [29] R. Krustev and H. Muller, An apparatus for the measurement of the gas permeability of foam films, *Rev. Sci. Instrum.* **73**, 398 (2002).
- [30] G. Cardano, *Ars Magna or the Rules of Algebra* (Dover, Oxford, UK, 1545).
- [31] L. Keiser, P. Marmottant, and B. Dollet, Intermittent air invasion in pervaporating compliant microchannels, *J. Fluid Mech.* **948**, A52 (2022).
- [32] Q. Magdelaine-Guillot de Suduiraut, *Hydrodynamique des films liquides hétérogènes*, Ph.D. thesis, Sorbonne Université, Paris, France (2019).
- [33] S. van Loo, S. Stoukatch, M. Kraft, and T. Gilet, Droplet formation by squeezing in a microfluidic cross-junction, *Microfluid. Nanofluid.* **20**, 146 (2016).
- [34] T. Ward, M. Faivre, M. Abkarian, and H. Stone, Microfluidic flow focusing: Drop size and scaling in pressure versus flow-rate-driven pumping, *Electrophoresis* **26**, 3716 (2005).
- [35] G. Ginot, F. S. Kratz, F. Walzel, J. Farago, J. Kierfeld, R. Hohler, and W. Drenckhan, Pressure-deformation relations of elasto-capillary drops (droploons) on capillaries, *Soft Matter* **17**, 9131 (2021).